

## Research Paper

# Using near-infrared enhanced thermozyyme and scFv dual-conjugated Au nanorods for detection and targeted photothermal treatment of Alzheimer's disease

Dongni Liu\*, Wei Li\*, Xiaoyu Jiang, Shuju Bai, Jiyang Liu, Xutong Liu, Yuhua Shi, Ziyu Kuai, Wei Kong, Renjun Gao<sup>✉</sup> and Yaming Shan<sup>✉</sup>

National Engineering Laboratory for AIDS Vaccine, Key Laboratory for Molecular Enzymology and Engineering of Ministry of Education, School of Life Science, Jilin University, Changchun, 130012, China

\* These authors contributed equally to this work.

✉ Corresponding authors: Yaming Shan (YS) and Renjun Gao (RG). E-mail: shanyam@jlu.edu.cn (YS) and gaorj@jlu.edu.cn (RG)

© Ivyspring International Publisher. This is an open access article distributed under the terms of the Creative Commons Attribution (CC BY-NC) license (<https://creativecommons.org/licenses/by-nc/4.0/>). See <http://ivyspring.com/terms> for full terms and conditions.

Received: 2018.10.13; Accepted: 2018.12.26; Published: 2019.04.12

## Abstract

Investigation of targeting inhibitors of A $\beta$  aggregation, heme-A $\beta$  peroxidase-like activity and efficient detectors of A $\beta$  aggregation, are of therapeutic value and diagnostics significance for the treatment of Alzheimer's disease (AD). Due to the complex pathogenesis of AD, theranostics treatment with multiple functions are necessary. Herein we constructed the NIR absorption property of gold nanorods (GNRs) loaded with single chain variable fragment (scFv) 12B4 and thermophilic acylpeptide hydrolase (APH) ST0779 as a smart theranostic complex (GNRs-APH-scFv, GAS), which possesses both rapid detection of A $\beta$  aggregates and NIR photothermal treatment that effectively disassembles A $\beta$  aggregates and inhibits A $\beta$ -mediated toxicity.

**Methods:** We screened targeting anti-A $\beta$  scFv 12B4 and thermophilic acylpeptide hydrolase as amyloid-degrading enzyme, synthesized GAS gold nanorods complex. The GAS was evaluated by A $\beta$  inhibition and disaggregation assays, A $\beta$  detection assays, A $\beta$  mediated toxicity assays *in vitro*. *In vivo*, delaying A $\beta$ -induced paralysis in AD model of *Caenorhabditis elegans* was also tested by GAS.

**Results:** *In vitro*, GAS has a synergistic effect to inhibit and disassociate A $\beta$  aggregates, in addition to decrease heme-A $\beta$  peroxidase-like activity. In cultured cells, treatment with GAS reduces A $\beta$ -induced cytotoxicity, while also delaying A $\beta$ -mediated paralysis in CL4176 *C.elegans* model of AD. Furthermore, the photothermal effect of the GAS upon NIR laser irradiation not only helps disassociate the A $\beta$  aggregates but also boosts APH activity to clear A $\beta$ . The GAS, as a targeting detector and inhibitor, allows real-time detection of A $\beta$  aggregates.

**Conclusion:** These results firstly highlight the combination of scFv, APH and nanoparticles to be theranostic AD drugs. Taken together, our strategy provides a new thought into the design of smart compounds for use as efficiently therapeutic and preventive agents against AD. Moreover, our design provides broad prospects of biomedical strategy for further theranostics application in those diseases caused by abnormal protein.

## Introduction

Alzheimer's disease (AD) is the most common neurodegenerative disorder, which affects at least 30 million people currently and is estimated to affect more than 106 million people by 2050 [1]. The

pathological indicator of AD is the accumulation of intracellular neurofibrillary tangles (NFT) and extracellular senile plaques (SP) [2]. The plaques are primarily composed of amyloid-beta (A $\beta$ ) peptides

containing 39–43 amino acids, which are generated by the cleavage of the transmembrane amyloid precursor protein (APP) named  $\beta$ - and  $\gamma$ -secretases [3]. Despite the full molecular mechanisms of AD pathogenesis remain unclear, overwhelming evidence indicates that  $A\beta$  neurotoxicity, which is strongly linked with the aggregation of  $A\beta$  monomers into neurotoxic oligomers or fibrils, is a common pathway and plays a pivotal role in the development of AD [4]. Therefore, theranostic strategies targeting  $A\beta$ -induced neurotoxicity are an attractive approach to treat AD [5, 6].

The steady-state levels of  $A\beta$  are largely regulated by the rate of protein production and clearance [7]. In brain tissue samples from AD patients,  $A\beta$  degradation is notably decreased, thus altering this equilibrium, leading to excessive  $A\beta$  peptide accumulation.  $A\beta$  aggregation in the hippocampus results in not only synaptic dysfunction but also neuronal cell death [8]. To date, there have been three main therapeutic strategies used to target  $A\beta$ -mediated neurotoxicity: reducing  $A\beta$  production [9], inhibiting  $A\beta$  aggregation [10], and increasing  $A\beta$  clearance rate [11]. Indeed, it has been reported that some agents would inhibit  $A\beta$  aggregation and disassemble preformed  $A\beta$  fibrils, resulting in decreased neurotoxicity. These agents include amyloid-degrading enzymes (ADEs) [12], monoclonal antibodies (mAbs) [13, 14], and nanoparticles (NPs) [15].

Currently, at least 20 different proteins are considered to be ADEs, including acylpeptide hydrolase (APH), insulin-degrading enzyme (IDE), neprilysin and endothelin converting enzyme, all of which have been reported to regulate secreted  $A\beta$  levels. For example, human APH, originally reported to hydrolyze polypeptides consisting of 30–50 amino acids, was found to degrade  $A\beta$  monomers, especially the toxic soluble oligomers. While human APH would appear to be an ideal means of regulating  $A\beta$  levels, this enzyme is not suitable for further drug development on its own on account of its low expression and loss of enzyme activity after purification. Hence, one of the current research directions is to screen stable and efficient ADEs.

In addition to ADEs, mAbs have also been used to target  $A\beta$  levels and toxicity. In fact, various mAbs have been tested in clinical trials, but most have failed owing to their accompanying side effects [13, 14]. Furthermore, scfv binds  $A\beta$  with a high specificity and while this inhibits  $A\beta$  accumulation, it does not eradicate the  $A\beta$ . This means that aggregation of the toxic proteins is only temporary blocked but can occur again, thereby limiting the effectiveness of mAbs in treating AD.

In recent years, the emerging development of nanomaterials offers a suitable scaffold for the combination of various drug treatments. NPs possess specific physiochemical properties almost completely different from those of macroscopical matter and have the capability to penetrate the blood brain barrier (BBB) because of their small nanometer dimensions [16]. A variety of NPs, such as rare earth NPs [17], chitosan NPs [18], magnetic NPs [19], polymeric NPs [15], have been applied to AD treatment, with varying success that largely depends on the drugs used in combination with the scaffolds. In addition to the use of ADEs, mAbs, and NPs, local heat generation (hyperthermia) is also an efficient strategy to dissolve  $A\beta$  deposits. Currently, photothermal treatment of nanoparticle is widely used as an invasive, non-toxic cancer therapeutic strategy, in which intracorporal organs are exposed to high temperatures to promote the selective elimination of abnormal cells [20, 21]. Furthermore, previous research indicates that graphene oxide, with high optical absorbance of the near infrared (NIR) light, can be utilized to photothermally disassemble  $A\beta$  deposits [22]. Other temperature-altering technologies, such as ultrasound, radio-frequency, and inductive microwave antennae, which were developed to heighten the temperature of a specific tissue but require a high frequency, also have an unexpected hyperthermic effect in the surrounding tissues [23, 24]. In contrast, laser irradiation in the NIR region penetrates peripheral tissues at an adequate intensity and high spatial accuracy to induce local hyperthermia [25]. According to the current investigation, only carbon-based nanostructures [26] and gold-based NPs [27] have the high optical absorption in the NIR region for photothermal therapy.

It is important to note that the clinical application of these agents, ADEs, mAbs, NPs, and hyperthermia, is limited by their respective shortcomings, which include only having a moderate inhibitory effect or weak disaggregation ability, low targeting properties, and/or biotoxicity. Furthermore, inhibiting  $A\beta$  monomer fibrillation or increasing  $A\beta$  fibril dissociation into monomers alone are inadequate as doing so has been shown to invoke heme- $A\beta$  complex formation, which may play a significant role in the onset of AD [28, 29]. This complex exhibits peroxidase-like activity, which catalyzes the oxidation of 3,4-dihydroxyphenylalanine and serotonin by reactive oxygen species (ROS). In order to overcome these obstacles for current AD treatments, it is essential to devise a multifunctional complex integrating the respective

benefits of each various reagent for the efficient theranostic of AD.

Therefore, the synergistic effect of the combine of ADEs, mAbs and NPs with photothermal treatment may be an efficient strategy of AD theranostics. In this study, we prepared a multifunctional complex that integrates the properties of an ADE (thermophilic APH ST0779), a single chain variable fragment (*scFv* 12B4), and a gold nanorod scaffold, designated GNRs-APH-*scFv* (GAS). Thermophilic APH ST0779 was cloned from thermophilic archaea *Sulfolobus tokodaii* as the ADE and expressed in *E. coli* BL21. Thermozyyme ST0779 is both highly stable and highly expressed [30]. This APH also exhibits higher activity levels under hyperthermia conditions than normal enzymes. Thermozyyme ST0779, like some other ADEs, may recognize multiple cleavage sites in A $\beta$ , thus reducing its peroxidase-like activity. However, this action requires further investigation. This ADE primarily hydrolyzes small peptides, including A $\beta$  monomers, at an optimum temperature of 70°C but still exhibits moderate enzyme activity at low temperatures. Unfortunately, despite these advantages, the enzymatic clearance of preformed A $\beta$  fibrils by thermophilic APH is low. ST0779 itself also has a high probability of being degraded by proteases. Thus, owing to the complex physiological conditions and complicated pathological mechanisms underlying A $\beta$  neurotoxicity, it is unlikely that this ADE can be used as an efficient treatment by itself.

We, therefore, also included *scFv* 12B4, which is constructed from mAbs, in the GAS complex. Small molecular antibodies, such as *scFv*, are one of the most promising immunotherapies [31-33]. Indeed, most mAbs recognize and bind all forms of A $\beta$ , and *scFv* in particular is prone to binding to A $\beta$  oligomers and fibrils. Previous studies indicate that A $\beta$  monomers may be of physiological significance to nerve cells in healthy individuals, so an antibody that exclusively recognizes A $\beta$  oligomers and A $\beta$  fibrils rather than the monomers is an ideal agent for AD treatment. Furthermore, it has also been shown that application of an anti-A $\beta$  antibody in the periphery can alter and/or regulate the dynamic balance of A $\beta$  between the cerebrum and sanguis, which plays an indirect role in transporting A $\beta$  out of brain and lightening the cerebrum load of A $\beta$ . However, while this indirect effect is beneficial, the most efficient mode of treatment is to across the blood brain barrier (BBB) and directly inhibit or moderate A $\beta$  aggregation and cytotoxicity. This is one advantage of *scFv*, which can penetrate the BBB due to its low molecule weight. *scFv* also decreases the probability of triggering a complement cascade reaction or inflammation because it lacks an Fc domain. The risk of microglial

overactivation induced by the phagocytosis of the A $\beta$ -*scFv* complex is also reduced. Moreover, compared to high molecular weight mAbs, the small size of *scFv* makes it easier for this mAb to approach and bind the A $\beta$  residues that contribute to their abnormal accumulation. However, *scFv* 12B4 treatment still has insurmountable shortcomings, such as a short half-life and possible protease degradation, that prevent it from being effective when used alone, hence its combination with thermophilic APH ST0779 in our complex.

To further aid the effectiveness of this traditional drug combination of thermophilic APH ST0779 and *scFv* 12B4, we also utilized gold nanorods (GNRs), one type of gold nanoparticle (AuNP), as a loading scaffold to construct our multifunctional protein-NP complex. Compared to other NPs, AuNPs are considered to be an excellent candidate for biomedical applications because of their outstanding biocompatibility, long term stability, optical properties, and ease of functionalization and bioconjugation [34]. For example, both APH and *scFv* can be easily conjugated to the GNRs by incorporating any externally exposed cysteine residue in the proteins via conventional Au-S chemistry [35]. Moreover, immobilization to GNRs also enhances protein stability. AuNPs, especially GNRs, when used as a scaffold loaded with thermophilic APH ST0779 and *scFv* 12B4, also have a high optical absorbance in the NIR region with a tunable excitation spectrum. In fact, GNRs have been shown to absorb NIR photo energy more effectively than spherical AuNPs. Compared to traditional remedies, such as chemotherapies and radiotherapies, this type of photothermal therapy treatment has also been shown to have decreased side effects and elevated selectivity since only organs and tissues under light irradiation are treated, while the surroundings kept in the dark will not be influenced. Furthermore, the rapid conversion of optical energy by the GNRs generates hyperthermia that not only disaggregates A $\beta$  fibrils but also provide a heat source to activate the thermozyyme. Thus, thermozyyme-mediated peptide degradation *in vivo* can be controlled with NIR irradiation. As previously reported, this internal heating mode of GNRs is more efficient and increases enzyme activity compared to diffusion-limited water bath heating. Moreover, *scFv* conjugation to the GNRs also avoids non-specific heating, reducing injury to normal tissues.

Apart from these beneficial properties, GNRs also have distinct surface plasmon resonance (SPR) characteristics. They have two surface plasmon absorbance bands determined by their geometric size and shape, one that is associated with the longitudinal

wave in the NIR region and another that is associated with the transverse wave around 520 nm. The wavelength shifts noted for GNRs make them extremely appropriate for biosensing applications involving changes in dielectric characteristics in the proximity of the particles, including those mediated by solvents, adsorbates, and the interparticle distances within the GNRs [36, 37]. During A $\beta$  aggregate binding, the binding-induced assembly of the GAS leads to coupling of the GNR plasmon bands. This means that the GAS complex acts as not only as a multifunctional anti-A $\beta$  agent but also a sensitive bioprobe that can be used to detect A $\beta$  aggregates.

In summary, GAS possesses the simultaneous functions of detector and inhibitor. GAS acts as a simple detector without NIR, monitoring A $\beta$  aggregation by naked eyes. Once detected the aggregates and upon NIR irradiation then, the targeted GAS blocks A $\beta$ -mediated toxicity as an inhibitor, degrading A $\beta$ , inhibiting A $\beta$  aggregation, disassembling A $\beta$  fibrils and reducing A $\beta$ -mediated peroxidase activity. In other words, once A $\beta$  fibrillization is detected via the bioprobe function of GAS, NIR light was utilized to activate the entire system, leading to a synergistic removal of excessive A $\beta$ . To the best of our knowledge, this is the first report to prepare and test a smart complex using concomitant *scFv*, thermophilic ADE, and GNRs for the treatment of AD. Moreover, we believe that the therapeutic model of this drug combination has the potential application of theranostics in more diseases, which has more than one symptoms caused by abnormal protein, such as Parkinson's disease and Huntington's disease.

## Methods

### A $\beta$ preparation

A $\beta$ 1-40 fragments were purchased from GenicBio Limited (lot no. P171125-GB20602). The peptides were first dissolved in 1,1,1,3,3,3-hexafluoro-2-propanol (HFIP) at a concentration of 1 mg/ml. The solution was shaken for 2 h at 4°C in a sealed vial for further dissolution. It was then stored at -20°C as a stock solution. Before use, the solvent HFIP was removed by evaporation under a gentle stream of nitrogen, and the peptide was dissolved in 20 mM Tris buffer, pH 7.4. A $\beta$ 1-40 oligomers and fibrils at 80  $\mu$ M were prepared from the freshly dissolved monomers for 3 and 8 days at 37°C, respectively, in 20 mM Tris, pH 7.4 buffer as previously described.

### GNRs synthesis

For GNRs formation, 7.5 mL of 0.20 M CTAB solution was added to 1.0 mL of 0.5 mM HAuCl<sub>4</sub>.

Then, 0.6 mL of ice-cold 0.01 M NaBH<sub>4</sub> was dropped in to the stirred solution, resulting in the formation of a brownish-yellow solution. After continuous stirring of this seed solution for 2 min, it was stored at 25°C. The growth solution was prepared by mixing 237.5 mL of 0.1 M CTAB, 1.5 mL of 0.01 mM AgNO<sub>3</sub>, and 10 mL of 0.01 M HAuCl<sub>4</sub> in a 500 mL flask. Approximately 1.6 mL of ascorbic acid (0.1 M) was then added dropwise to the mixture slowly until it became colorless, after which additional ascorbic acid was added (a quarter of the total number of droplets to that point). Finally, 2 mL of the seed solution was added to the growth solution at 27–30°C. The color of the solution changed within 10–20 min gradually. During the full process, the temperature of the growth medium was kept constant at 27–30°C.

### GAS complexes synthesis

The synthesized GNRs (10 mL aliquots) were centrifuged at 12500 rpm for 20 min to remove excess CTAB surfactant. The precipitate was dispersed in 8 mL of Milli-Q water after discarding the supernatant. Then, 0.2 M K<sub>2</sub>CO<sub>3</sub> solution was added while stirring to adjust the pH to 9. Following this step, 2.5 mL of 2 mg/ml thermozyyme ST0779 and 200  $\mu$ L of 100  $\mu$ M *scFv* 12B4 were mixed with the GNRs solution under vigorous stirring at room temperature. Protein conjugation was allowed to proceed for 12 h. To remove excess protein, this procedure was then followed by centrifugation at 8000 rpm for 10 min.

### ThT fluorescence measurements

The A $\beta$  aggregation kinetics were monitored with ThT dye, the fluorescence of which is dependent on the formation of amyloid fibrils. At various points during incubation (1, 2, 3, 4, 5, 6, and 7 days), aggregated A $\beta$ 1-40/GAS samples were irradiated with an NIR laser for 5 min before being diluted to a final concentration of 2  $\mu$ M (A $\beta$ 1-40 concentration) with aggregation buffer at pH 7.3 containing 10  $\mu$ M ThT for fluorescence measurements. The fluorescence signal (excitation at 444 nm) was recorded between 460 and 650 nm using 10 nm slits for both the emission and excitation measurements.

### Transmission electron microscopy (TEM)

A $\beta$ 1-40 monomers, oligomers, and fibrils (50 mM) in the presence or absence of GAS (50  $\mu$ g/mL) were irradiated for 5 min per day followed by incubation at 37°C for 2 days. The samples were dropped onto carbon-coated copper grids and incubated for 30 min. The samples were then adsorbed excess buffer with filter paper from the grids, after which the substrates were washed with deionized water three times. The samples were

observed on a transmission electron microscope (JEOL JEM-1011) operating at a voltage of 200 kV.

### **A $\beta$ -mediated peroxidase activity measurements**

An inhibition assay was performed as previously described. 3,3',5,5'-tetramethylbenzidine (TMB) was used as the substrate to measure peroxidase activity. Briefly, 10 mg of TMB was dissolved in 10 mL of AcOH/NaOAc buffer (1 M, pH 4.5) and 0.5 mL of glacial AcOH. This was followed by the dilution to 25 mL with water, and then 100  $\mu$ L, 30 vol H<sub>2</sub>O<sub>2</sub> was added. After mixing the solution, addition of 10  $\mu$ L of 0.05 mM sample was prepared for measurement. Kinetic traces were obtained by monitoring the increase of the 652 nm absorbance band over time.

### **A $\beta$ toxicity inhibition assay**

As for MTT assay, SH-SY5Y cells were plated at a density of 50000 cells per well on 96-well plates and cultured overnight. After addition of the prepared A $\beta$  and different dilution sample into the cell culture medium, the plates exposed to 808 nm NIR laser irradiation at a power density of 2 W cm<sup>-2</sup> for 5 min. After 24 h of incubation at 37 °C, each well was treated with MTT (5 mg/mL in 20  $\mu$  L) and incubated for another 4 h at 37 °C. After the Centrifugation to remove the supernatants carefully, DMSO (150  $\mu$  L) was added to each well of the plates. Cell viability was obtained by measuring the absorbance values of each well at 490 nm using an ELISA reader (Bio-Rad, USA).

### **C. elegans maintenance and treatment**

In the study, the transgenic strain *Caenorhabditis elegans* CL4176 [smg-1(cc546ts);dvIs27(pAF29+pRF4)] was used as an AD model. Transfected CL4176 nematodes constitutively produce A $\beta$ 1-42 in the muscles of their body walls. *E.coli* OP50 was fed as a food source to the worms and the worms were propagated at 16°C on solid nematode growth medium (NGM). To obtain age-synchronized worms, hermaphroditic CL4176 worms were transferred to fresh NGM plates reaching maturity (3 days old). After another 4 to 6 h incubation, the mature CL4176 worms were removed to leave the eggs. Isolated hatchlings were then cultured on new NGM plates at 16°C.

### **C. elegans paralysis assay**

After age synchronization, worms were incubated at 16°C on fresh NGM plates (35 mm  $\times$  10 mm, 60 worms per plates). In the experimental group, the worms were fed GAS (40  $\mu$ M per plate), while those in the control group were fed normally. Upon reaching the L3 larval stage, NIR laser irradiation was

performed for 1 min, and then the worms were placed in a 16°C incubator. Paralysis was measured at the L4 stage at 25°C, which normally induces A $\beta$ 1-42 expression. The nematodes who only moved their heads or did not move at all when gently touched with a platinum loop were considered paralyzed. A total of four independent trials were performed.

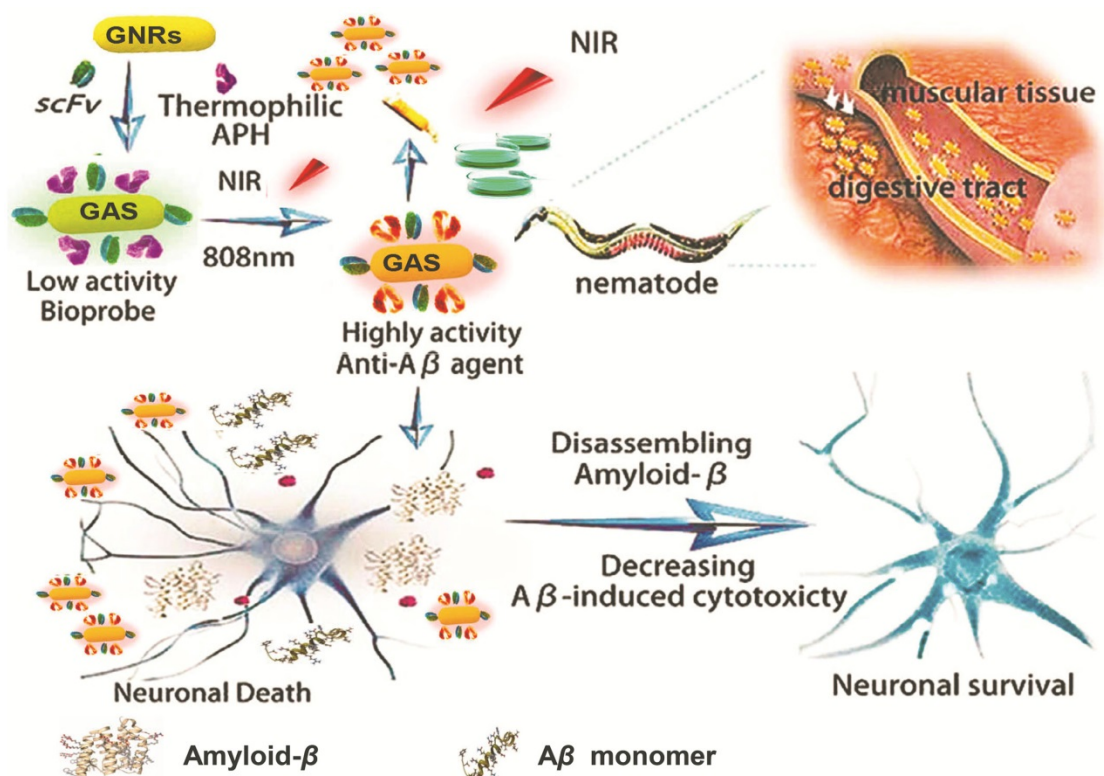
## **Results and Discussion**

### **GAS composition**

Scheme 1 shows the construction of our multifunctional complex that incorporates GNRs loaded with thermophilic APH ST0779 and *scFv* 12B4 (GNRs-APH-*scFv*, GAS). In theory, upon laser exposure (808 nm), the GNRs will generate local heat to activate the thermozyyme and dissociate the A $\beta$  fibrils. As thermozyyme ST0779 effectively hydrolyzes A $\beta$  monomers and *scFv* 12B4 selectively binds to A $\beta$  oligomers and fibrils and inhibits A $\beta$  aggregation, treatment with this complex will affect A $\beta$  toxicity regardless of the morphology of the fragments, ideally leading to a complimentary and synergistic effect during AD treatment.

### **GAS preparation**

GNRs were synthesized by a seed-mediated surfactant-directed method as previously reported [38], whose aspect ratio is approximately 3.6. GNR morphology was characterized by transmission electron microscopy (TEM; Figure 1A). Our analysis indicates that the average length of the GNRs was about 30 nm, with an average width of 8.3 nm. Prior to constructing the multifunctional GAS complex, we measured photothermal conversion efficiency of the GNRs at different concentrations upon 808 nm NIR laser irradiation at varying power. By adjusting the laser power and/or GNR concentration, we were able to obtain the exact desired temperature (Figure 1C and 1D) within the range of 20-63°C. The thermozyyme ST0779 and *scFv* 12B4 were obtained and purified as previous reported [30, 32]. For GAS complex construction, GNRs were mixed with specific concentrations of thermozyyme ST0779 and *scFv* 12B4. During this reaction, the thiol sulfur atoms of cysteine form polar covalent Au-S bonds that attach the enzyme to GNR surface via self-assembly. Moreover, the loading concentrations of APH and *scFv* were determined by the degrading or inhibitory effect on A $\beta$  in an *in vitro* experiment (Figure S1). Within the allowable ranges, beyond which will lead to the aggregation of GAS, the optimum concentrations of APH and *scFv* is 0.46mg/ml and 18 $\mu$ M, respectively. The complexes were then characterized by TEM (Figure S2), UV-vis spectroscopy (Figure 1B), and FTIR spectroscopy (Figure S3). TEM indicates that the



**Scheme 1.** Schematic representation of GAS used for AD treatment. The schematic illustration of the preparation of GAS. The GAS with high NIR absorption used for AD diagnosis and treatment.

morphology of GAS did not change much compared to that of GNRs. In our UV-vis spectroscopy analysis, the peak representing the GNRs shows a red shift from 722 nm to 707 nm and a blue shift from 521 nm to 526 nm, and the appearance of a characteristic peak at approximately 280 nm indicates peptide conjugation. Furthermore, in our FTIR spectroscopy analysis, the weakening of the peak at  $2600\text{ cm}^{-1}$  that corresponds to the cysteine thiol groups of the two proteins confirms that these groups have formed Au-S bonds during attachment to the GNR surfaces. Together, these analyses reveal that the major functional groups in the APH and *scFv* also appeared in the GAS complex, indicating successful conjugation of both agents to the GNR surface. Further, it was also necessary to evaluate any conjugation-mediated changes in enzyme activity. A small peptide containing three alanines was used as a substrate to detect enzymatic activity from 20–40°C. Intriguingly, the activity of the thermozyms bound to the GNRs was increased upon NIR laser irradiation compared to that of free thermozyms activated by water bath (Figure S4). By adjusting the laser power, the enzymatic activity of GAS can be regulated within the range of 30–60°C (Figure S5). This indicates that the two different heating methods may alter enzyme activity differently at the microcosmic level but similarly at the macrocosmic level [39]. Notably, the

increased temperature leading to increased thermozyms activity was local and the overall temperature of the solution was not increased (data not shown). These findings are consistent with previous reports. Moreover, we also evaluated the stability of thermozyms ST0779 and the *scFv* 12B4 after conjugation to the GNRs (Figure S6). The stability of free APH dramatically decreased and was totally degraded in approximately 60 min. In contrast, GAS was found to be significantly more stable, with 46.2% intact protein remaining after 60 min. Moreover, the zeta potentials of the GAS complex and GNRs were  $-15.8 \pm 3.1\text{ mV}$  and  $-30.9 \pm 0.4\text{ mV}$ , respectively. These data indicate that the complex has a relatively high colloidal stability and will not easily adsorb the majority of proteins *in vivo* due to its negative charge.

Notably, the surface charge of NPs, especially negative charge, plays a significant role in the inhibition of A $\beta$  fibrils formation [40–42]. When incubated with the negatively charged GAS, despite the absence of NIR irradiation, the charge carried by the material itself would depress the formation of A $\beta$  aggregates due to the electric attraction of the positively charged residues responsible for the fibrils formation irrespective of the material composition. This assumption was also proved in the subsequent experiments.

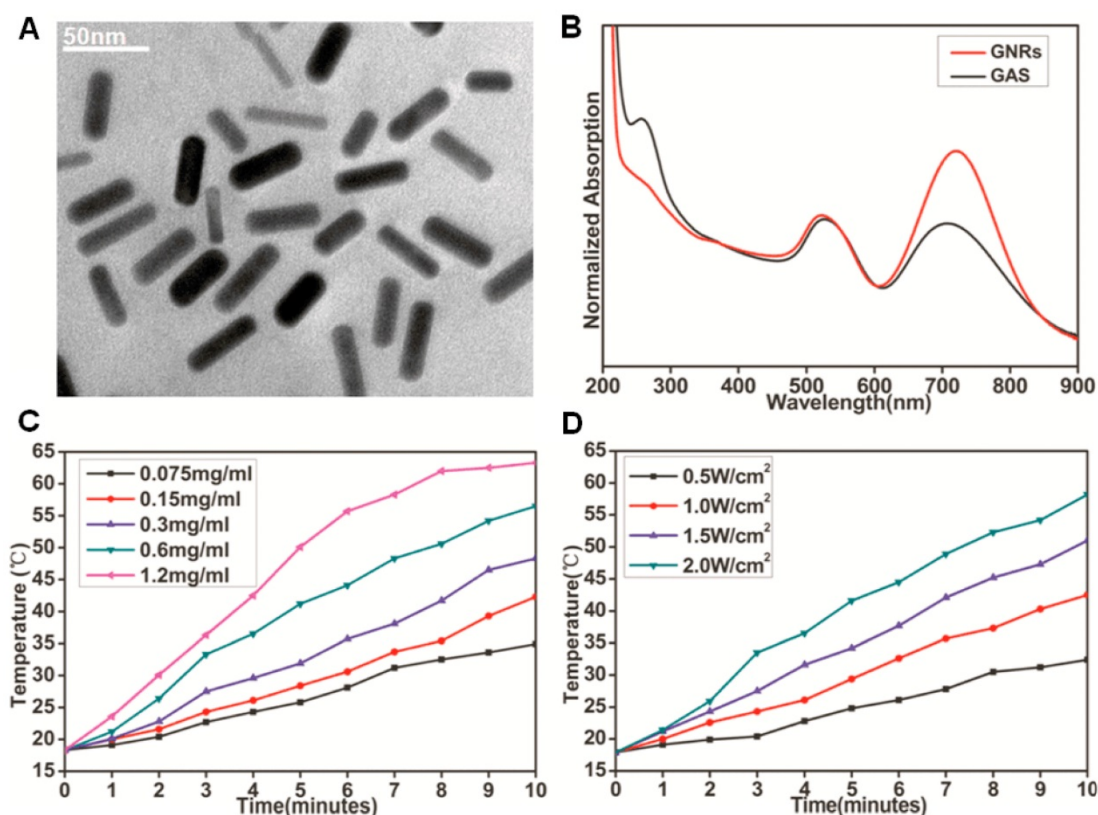


**Figure 1.** Characterization of GNRs and GAS. (A) TEM image of as synthesized GNRs. (B) UV-Vis absorption spectrum of GNRs and GAS; NIR-induced heat generation of GAS aqueous solution (C) different concentrations at the same power densities of  $2\text{W cm}^{-2}$ , (D)  $0.6\text{mg mL}^{-1}$  at different power densities.

## A $\beta$ aggregate biosensing

To monitor A $\beta$  fibrillogenesis using the GAS complex as a bioprobe, A $\beta$ 1-40 was selected for the peptide model, as its distinct effects on neurons have been clearly elaborated [43]. Most studies utilizing the localized surface plasmon resonance (LSPR) mechanism of GNRs as bioprobes have been based on the attachment-induced aggregation of the NPs. Theoretically, the oscillation of the plasmons from adjoining GNRs become coupled when the distance between the GNRs is almost equal to or even shorter than the binding radius, resulting the reduction of the vibration frequency [44]. This change is manifested as a shift in the absorbance bands from red region to longer wavelengths. Therefore, upon binding of *scFv* 12B4 in the GAS complex to A $\beta$ , A $\beta$  aggregation can be visualized via these shifted bands. Notably, the addition of A $\beta$  monomers with the random coil conformation could not induce GAS aggregation. However, the presences of A $\beta$  fibrils could be recognized and caused the formation of a close reticulation between the *scFv*-conjugated GNRs. In the presence of different concentrations of A $\beta$  fibrils, the transverse plasmon peak of GAS was red-shifted, while the longitudinal one was blue-shifted (Figure S7A). Due to the insolubility of A $\beta$  fibrils and the targeting ability of *scFv*, GAS precipitated with A $\beta$

together accompanying by fibrils formation, resulting in a transparent solution. These typical changes in the absorbance spectra can be attributed to binding-induced GAS aggregation, the degree of which appears to be associated with A $\beta$  fibrils concentration.

Furthermore, the absorbance characteristics of GAS in the absence or presence of A $\beta$  fibrils was also utilized to monitor the dynamics of A $\beta$  fibrillogenesis *ex situ* and to construct a system combining diagnostic and therapeutic functions. A $\beta$  incubated for different lengths of time was mixed with GAS ahead of spectral measurement. In Figure 2A, the absorption bands exhibited gradient changes and these changes were associated with the incubation time. Furthermore, the color of the solution became transparent from violet as the aggregation process progressed, while the GAS itself was not changed (Figure 2B), indicating that A $\beta$  fibrillogenesis can be visualized with the naked eye in this multifunctional system. Upon NIR laser irradiation, the shift of plasmon bands was recovered to varying degrees for samples incubated up to three days (Figure S7B and S7C), suggesting that the multifunctional GAS complex can be used to monitor A $\beta$  aggregation in real time and treat it via NIR irradiation in that same time period.

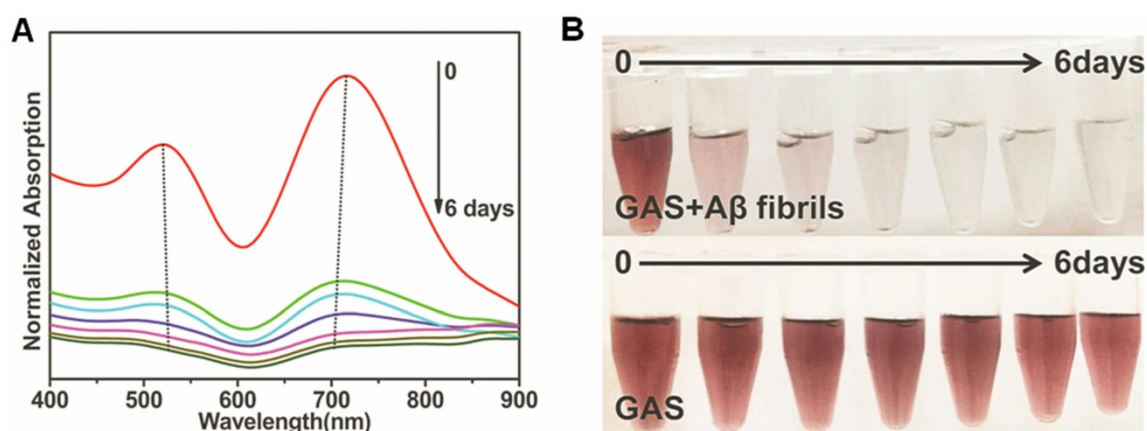


**Figure 2.** A $\beta$  aggregate biosensing by GAS. (A) A $\beta$  fibrillogenesis process monitored by the absorbance spectrum of GAS. The final concentration of A $\beta$  and GAS were 5 $\mu$ M and 400 $\mu$ g mL<sup>-1</sup>. (B) Colorimetric response of GAS in the presence or absence of A $\beta$  in HEPES buffer measured at different incubation time from 0 to 6 days. The final concentration of A $\beta$  and GAS were 5 $\mu$ M and 400 $\mu$ g mL<sup>-1</sup>.

### Degradation, inhibition, and disaggregation testing

To verify the inhibitory effect of GAS on the aggregation of A $\beta$  monomers, a common *in vitro* thioflavin T (ThT) fluorescence assay has been conducted [17]. The content of  $\beta$ -sheet aggregation structure of A $\beta$  depends on the degree of A $\beta$  fibrilization which increases with incubation time. ThT is an extrinsic fluorescent dye, which binds to the  $\beta$ -sheet structure of A $\beta$  aggregates. Upon binding, the fluorescence intensity increased corresponding with the raised binding level. Accordingly, the synergistic effect of the GAS complex on A $\beta$  fibrillogenesis was quantitatively evaluated by measuring ThT fluorescence intensity at 480 nm as well as excitation at 444 nm. Despite the significant absorption of GNRs at this emission wavelength may affect ThT fluorescence, the concentration chose to ensure *in vivo* application is very low, which would not change fluorescence intensity (Figure S8). When fresh A $\beta$  was incubated alone at 37°C, the ThT fluorescence formed a sigmoidal curve as a reflection of incubation time in accordance with the nucleation-dependent polymerization model. When A $\beta$  was incubated with 40  $\mu$ g/mL GAS and NIR laser irradiated for 5 min per day, the ThT fluorescence increased extremely slowly and the total was reduced by approximately 72% compared to that of A $\beta$  incubated without GAS (Figure 3A-a). This indicates that A $\beta$  fibrils formation was suppressed by GAS treatment. Moreover, we also tested the effects of APH and *scFv* alone as well as combinations of APH and *scFv*, GNRs-APH, and GNRs-*scFv* on A $\beta$  fibril formation and aggregation to confirm the synergistic effects of the complex. When used alone, the APH completely lost its inhibitory effects after day 4, likely owing to protein denaturation or inactivation. However, conjugation to GNRs offered the necessary heat and stability to

preserve APH enzyme activity, and the fluorescence intensity was reduced by 14%. Similarly, the GNR-modified *scFv* had increased stability and avoided the denaturation observed for the *scFv* alone. While the GNR-bound agents were more effective than the unbound agents, the decline in ThT fluorescence observed in the presence of the GAS complex exceeded the total of these individual fluorescence reductions observed for the respective components, indicating an effective synergistic effect and the significant role of negative charge in A $\beta$  aggregation inhibition.

Subsequently, we also evaluated the inhibitory and disassembling effect of GAS on A $\beta$  oligomers, which is the most toxic form of A $\beta$ . A $\beta$  monomers were preincubated alone for 3 days at 37°C in order to obtain A $\beta$  oligomers, which would be continuously aggregating to form A $\beta$  fibrils over the next few days. In the presence of GAS under the same conditions for an additional 7 days, the fluorescent intensity was reduced by 74% compared to that of A $\beta$  oligomers incubated alone (Figure 3A-b). As for APH, *scFv* and the various combination mixtures, the fluorescence intensity trended to decline slightly in the first 4 days and then ascended. The ability of APH to degrade A $\beta$  oligomers is likely much weaker than its ability to degrade A $\beta$  monomers, and the stability of both APH and the *scFv* worsens over time. The degrading capabilities and inhibitory effects of APH and *scFv* decreased as the fibrilization process continued. In other words, in the last few days of the experiment, the rate of A $\beta$  fibril formation from the oligomers was higher than the clearance rate mediated by APH and the inhibitory effects of *scFv*. However, after conjugation with GNRs, the ThT fluorescence of the GNR-APH- and GNR-*scFv*-treated samples decreased by 39% and 27%, respectively. Thus, comparing to the solo agents and even the GNRs-bound agents, our

multifunctional GAS complex had the same synergistic effect in the inhibition of A $\beta$  oligomer accumulation as it did for A $\beta$  monomers. Moreover, due to the negative charge, the inhibitory and disassembling effects of GAS on A $\beta$  oligomers were even better than those on A $\beta$  monomers with respect to the charged protein residues that are responsible for  $\beta$ -sheet.

Furthermore, to evaluate the synergistic effect of GAS in disaggregating preformed A $\beta$  fibrils, the A $\beta$  monomers were preincubated for 7 days at 37°C, and then GAS was added and NIR irradiated. After incubation for another 7 days, the amount of A $\beta$  fibrils was measured. Our results show that GAS effectively dissociates A $\beta$  fibrils, as evident by the 56% reduction in fluorescent intensity (Figure 3A-c). In the control experiment, APH had almost no effect, while *scFv* had a weak effect on dissociating pre-formed A $\beta$  fibrils. However, when conjugated to GNRs, the ThT fluorescence of the GNRs-enzyme- and GNRs-*scFv*-treated samples decreased by approximately 24% and 27%, respectively. This

indicates that the GAS-mediated hyperthermia contributed to the disassembly of A $\beta$  fibrils the most, and treatment with the complex once again decreased fluorescence intensity in a synergistic manner. Notably, the negative charge of GAS can efficiently inhibit the depolymerization products of A $\beta$  fibrils, such as oligomers and short peptides, to form aggregates a second time. Meanwhile, *scFv* and photothermal effect could both assist in the disassociation of oligomers and short fibers, which is conducive to a thorough removal of A $\beta$  by APH catalysis. In summary, GAS exhibits synergistic effects on the inhibition of A $\beta$  monomer and oligomer aggregation as well as during the dissociation of pre-formed A $\beta$  fibrils.

To confirm the above results and further study the morphological changes of the A $\beta$  peptides upon NIR laser irradiation, TEM was used. As shown in Figure 3B-a, 3B-c, and 3B-e, the classical A $\beta$  peptide morphology was observed in prepared samples of A $\beta$  monomers, oligomers, and fibrils [45]. While the A $\beta$  monomers cannot be observed clearly due to the

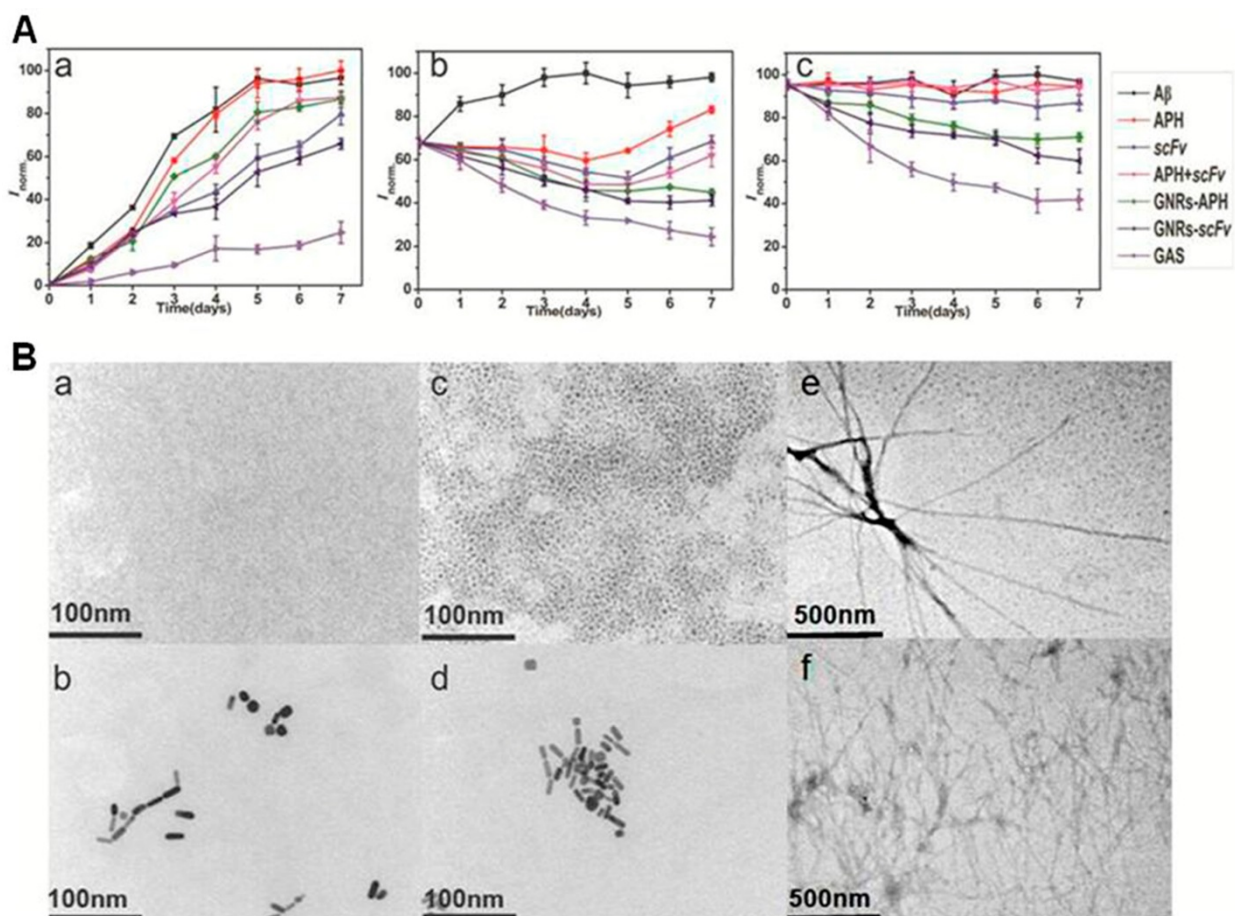


**Figure 3.** Degradation, inhibition and disaggregation effects of GAS against A $\beta$ . (A) Fibrillation kinetics of A $\beta$  as monitored by the development of thioflavin T binding in the absence of GAS (■) or in the presence of APH (●), *scFv* (▲), combination of APH and *scFv* (▼), GNRs-APH (◆), GNRs-*scFv* (◄) or GAS (►) for monomers (a), oligomers (b) and fibrils (c). (B) Inhibition and disaggregation of A $\beta$  aggregates by GAS as monitored by TEM. A $\beta$  monomers in the absence of GAS (a) or in the presence of GAS (b), A $\beta$  oligomers in the absence of GAS (c) or in the presence of GAS (d) and A $\beta$  fibrils in the absence of GAS (e) or in the presence of GAS (f) after incubation for 7 days upon NIR laser irradiation for 5 minutes per day.

resolution ratio of the TEM, the oligomers appear to be spherical with a height of 1 nm to 6 nm. Further, the A $\beta$  fibrils form helical fibers with a height of 10 nm and maximum lengths greater than 1  $\mu$ m. All of these A $\beta$  intermediate morphologies are consistent with previous reports. In contrast, when A $\beta$  monomers were incubated with GAS upon NIR laser irradiation, nothing but the multifunctional complexes could be observed (Figure 3B-b). After incubating for another 2 days, the observed results remained the same (Figure S9), indicating that GAS likely has a prophylactic effect. Despite removal of GAS from the incubated solution, A $\beta$  oligomers or fibrils would not form again for 7 days, indicating the high clearance of GAS (Figure S10). In the samples of A $\beta$  oligomers incubated with GAS, most of the spherical A $\beta$  peptides were gone (Figure 3B-d). Similarly, after NIR laser irradiation, small and amorphous species were observed in the GAS-treated samples of A $\beta$  fibrils. Moreover, some of the multifunctional complexes, observed as black beads, were found close to the ends of various fibrils (Figure 3B-f). Thus, our TEM results intuitively support our earlier results and indicate that the complexes can effectively degrade A $\beta$  peptides, inhibit A $\beta$  assembly, and disaggregate A $\beta$  fibrils.

To better understand the multifunctional effects of GAS on the three forms of A $\beta$  peptides, the levels of A $\beta$  degradation, inhibition, and dissociation were also investigated by western blotting (Figure S11). A $\beta$  peptides from the stock solution adopted a monomeric form without incubation. After incubation, we observed multiple bands, indicating the formation of oligomers and fibrils. In contrast, after incubating with GAS for 7 days, the A $\beta$  monomers were strongly degraded and the formation of A $\beta$  aggregates was significantly inhibited, as evident from the weak monomer and aggregate bands. In the presence of GAS, the bands for the oligomers and fibrils were also weaker, demonstrating that GAS degraded, disassembled, and inhibited the A $\beta$  oligomers and fibrils. Moreover, both A $\beta$  oligomers and fibrils would produce a certain amount of monomers under the depolymerization action of GAS, cyclic dichroism (CD) has been performed to analyze this action (Figure S12). The monomers has a negative peak near 200nm, demonstrating the random coil structure. However, after incubation with GAS upon NIR laser irradiation, the wave form of A $\beta$  monomers became disordered, indicating the destruction of the secondary structure. This disorder further demonstrate the incubation products would not form fibrils again regardless of whether GAS was removed or not. These results further support the analyses of our ThT and TEM

experiments and highlight the multifunctional and synergistic effects of GAS on various A $\beta$  peptides.

### A $\beta$ -induced toxicity detection *in vitro* and in cell culture

Previous studies have demonstrated that heme binds to soluble A $\beta$  peptides, resulting in the formation of heme-A $\beta$  complexes and heme deficiency [28]. As heme is required for normal biological functions, this can cause detrimental effects. Furthermore, the heme-A $\beta$  complexes also exhibits the activity of peroxidases, which catalytically oxidize neurotransmitters like serotonin, 4-hydroxyphenylpyruvic acid, and 3,4-dihydroxyphenylalanine by H<sub>2</sub>O<sub>2</sub>. In native human A $\beta$  peptides, both His13 and His14 can coordinate with the heme. Indeed, mutating or disrupting these residues prohibits heme binding, leading to loss of peroxidase activity [46]. Our HPLC-MS data indicate that thermophilic APH ST0779 can degrade A $\beta$  into small pieces via cleavage at various sites, including His13 and His14 (Figure S13). It is, therefore, possible that human APH may also function to reduce the ROS produced by the heme-A $\beta$  complex. Similar to previous studies, our data show that the heme-A $\beta$  complexes display remarkably improved peroxidase activity compared to free heme. However, when GAS was added to the reaction system and NIR irradiation was administered, the peroxidase activity decreased by approximately 48% (Figure 4A and Figure S14). In control experiments using APH alone or GNR-APH, the heme-A $\beta$  peroxidase activity decreased by approximately 22% and 36%, respectively. Interestingly, when *scFv* as well as the mixture of *scFv* and thermozyme were added to the solution, the peroxidase activity was also reduced by 21% and 33%. In summary, these results suggest that GAS acts as an efficient inhibitor of heme-A $\beta$  complex peroxidase activity and could be utilized as a multifunctional agent to treat AD.

Since GAS inhibits heme-A $\beta$  complex-mediated cellular stress while also degrading A $\beta$  monomers, inhibiting A $\beta$  accumulation, and disassembling A $\beta$  fibrils upon laser irradiation *in vitro*, it may also decrease A $\beta$ -mediated cellular toxicity. To evaluate this cellular function, we performed an MTT (3-(4,5-dimethylthiazol-2-yl)-2,5-diphenyltetrazolium bromide) assay to investigate cellular metabolism in SH-SY5Y cells. Notably, cells treated with A $\beta$  monomers, oligomers, and fibrils for 24 h had reduced cell viability (89.7%, 49.9%, and 76.1%, respectively) compared to untreated controls (Figure 4B). These data are consistent with the conclusion that A $\beta$  oligomers are the most toxic form. In the presence of gradient concentrations of GAS and laser irradiation,

the survival of the cells treated with A $\beta$  monomers was increased to 99% (Figure 4Ba), while that of cells treated with A $\beta$  oligomers and fibrils were increased to 93% and 96% (Figure 4C and 4D). GAS-mediated cell survival also appears to be concentration dependent. Notably, cell viability was largely unaffected following treatment with A $\beta$  fibrils along with GAS in the absence of NIR laser irradiation or with GAS and NIR laser irradiation alone (no A $\beta$  treatment) (data not shown). Moreover, the survival of cells treated with A $\beta$  monomer was also increased when treated with APH and *scFv*. In fact, survival after these treatments was only slightly less than that observed for GAS, indicating that the complex as well as individual agents limit the cellular toxicity of A $\beta$  monomers. However, APH solo treatment barely had an effect on cells treated with A $\beta$  oligomers or fibrils. In summary, GAS and NIR laser irradiation treatment is not only efficient during *in vitro* experiments, but also decreases A $\beta$ -induced cytotoxicity in cultured cells.

### C. *elegans* paralysis assay

Based on our *in vitro* and cell culture results, we next evaluated the *in vivo* effects of GAS as an anti-A $\beta$  agent using *Caenorhabditis elegans* as a model

organism. The transgenic *C. elegans* strain CL4176 has been widely used to study and develop AD drugs as A $\beta$ 1-42 expression can be induced in the body wall muscles of larval worms via changes in environmental temperature (from the permission temperature of 16°C to the non-permission temperature of 25°C). This higher temperature inactivates the *smg-1* system, allowing translation of the stabilized transgene mRNA for human A $\beta$  and the subsequent development of rapid and progressive paralysis. As shown in Figure 5, the untreated control worms were almost completely paralyzed within 54 h after the temperature was increased, while treatment with GAS and NIR laser irradiation postponed paralysis to approximately 62 h. Notably, worms incubated with GAS but not administered NIR laser irradiation did not have any delay in paralysis. Moreover, the peak period of paralysis was 46~48 h (n = 14) for the control group and 50~52 hours (n = 11) in the GAS and NIR laser irradiation-treated group. To further observe these effects, videos were taken of the CL4176 worms (beginning at 46 h post-temperature change) in the presence or absence of GAS and NIR laser irradiation. In the untreated control group, most of the nematodes were inactive with rigid bodies

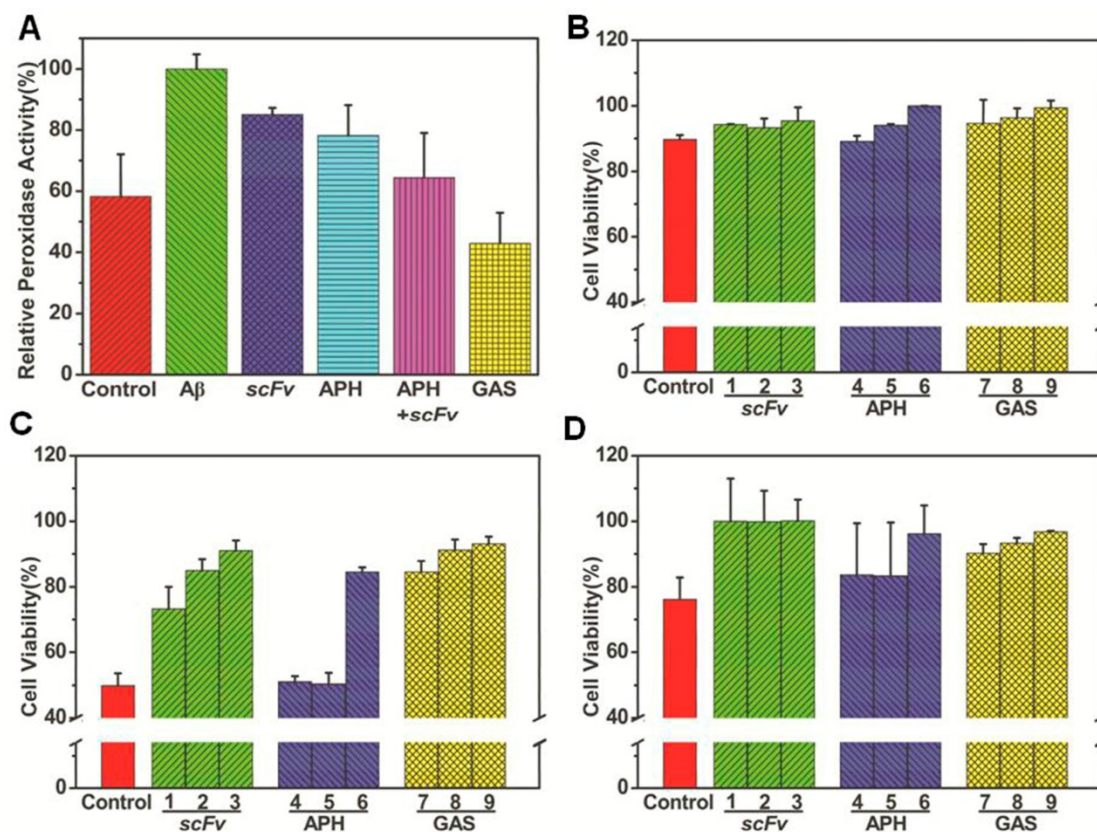


**Figure 4.** A $\beta$ -induced toxicity inhibited by GAS *in vitro* and in cultured cells. (A) Decrease of A $\beta$ -mediated peroxidase activity by GAS as monitored the increase of the 420nm absorption intensity after 1200 seconds for different heme-A $\beta$  complex inhibitors; Effect of different concentrations of APH, *scFv* and GAS on the cytotoxicity of A $\beta$  monomers (B), oligomers (C) and fibrils (D). The concentration of *scFv* equal to the equivalent of GAS was 75  $\mu\text{g mL}^{-1}$  (1), 150  $\mu\text{g mL}^{-1}$  (2) and 300  $\mu\text{g mL}^{-1}$  (3), the concentration of APH equal to the equivalent of GAS was 37.5  $\mu\text{g mL}^{-1}$  (4), 75  $\mu\text{g mL}^{-1}$  (5) and 150  $\mu\text{g mL}^{-1}$  (6), and the concentration of GAS was 125  $\mu\text{g mL}^{-1}$  (7), 250  $\mu\text{g mL}^{-1}$  (8) and 500  $\mu\text{g mL}^{-1}$  (9). The cytotoxic effect on SYHY5 cells was examined by MTT assay.

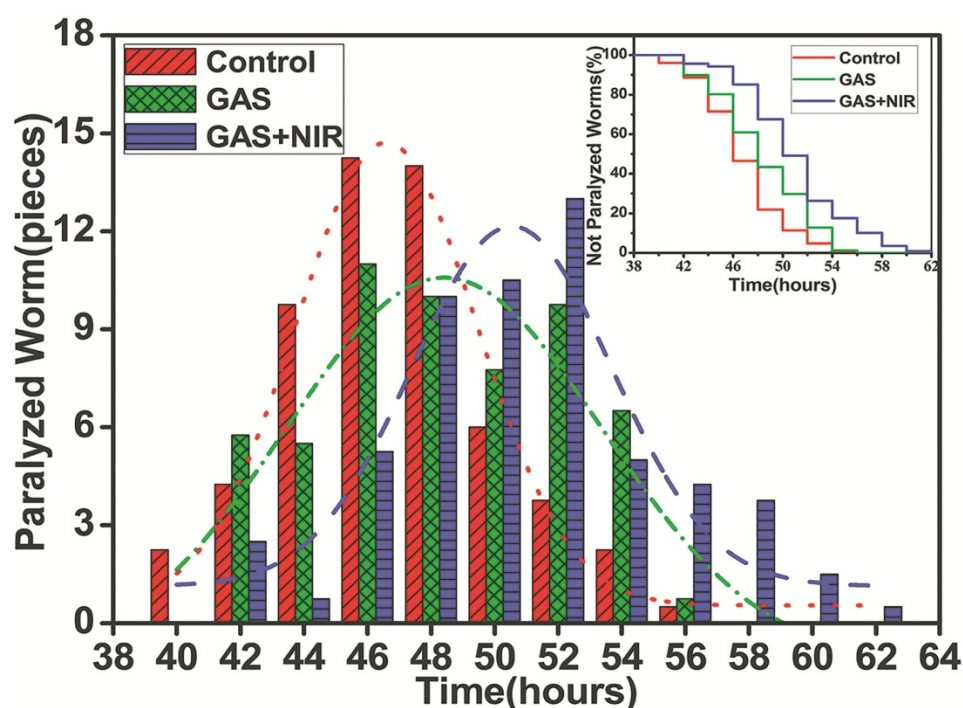


**Figure 5.** The effect of GAS upon NIR laser irradiation on the life span of transgenic strain CL4176. The number of nematodes paralyzed every two hours was fitted by normal distribution curves to indicate the peak period of paralysis. Kaplan-Meier survival curves of the transgenic strain CL4176 treated without (red) or with 500  $\mu\text{g mL}^{-1}$  GAS upon (blue) or not upon (green) NIR laser irradiation.

classified as “J” type, only moving their heads or not moving at all when gently touched (Video 1 and 2). However, in the experimental GAS/NIR-treated group, the nematodes were still active and would rapidly wriggle when gently touched, being classified as “C” type in the static state (Video 3 and 4). These data demonstrate that GAS plus NIR irradiation effectively extends the life span of *C. elegans* by reducing A $\beta$ -mediated toxicity and can be used as both a treatment and a preventive agent.

## Conclusion

The complicated pathogenesis of AD indicates that it requires comprehensive theranostic therapy with multifunctional agents. Based on this, we designed and synthesized the GAS complex as a novel smart anti-A $\beta$  agent, which not only detects A $\beta$  aggregates rapidly, but also efficiently disaggregates A $\beta$  aggregates and inhibits A $\beta$  mediated toxicity with NIR photothermal treatment. Our design integrates the unique NIR absorbance properties of GNRs with the efficient and stable A $\beta$  degrading ability of APH and the inhibitory as well as A $\beta$  targeting effects of *scFv*. The photothermal effect of the GNRs was also utilized to not only dissociate A $\beta$  deposits but also to enhance thermozyyme activity. This heating mode protects the thermozyyme from non-specific degradation by other peptides better than standard heating via water bath. Immobilization of APH and the *scFv* also increases their stability and confers

resistance to protease-mediated hydrolysis. With regards to treatment, our GAS has smart synergistic effects and degrades A $\beta$  monomers, inhibits A $\beta$  accumulation, and disaggregates A $\beta$  fibrils in addition to reducing A $\beta$ -mediated peroxidase activity. Importantly, this reduction in A $\beta$ -induced cytotoxicity was observed both *in vitro* and in cultured cells. GAS with NIR irradiation also appears to be an effective preventive AD drug in a *C. elegans* AD model. To our knowledge, this is the first study to integrate these three agents (APH, *scFv*, and GNRs) in one system for AD therapy. Taken together, our results provide new insight into the design of multifunctional protein-GNR conjugation systems for AD treatment.

## Abbreviations

AD: Alzheimer's disease; A $\beta$ : amyloid- $\beta$ ; GNRs: gold nanorods; *scFv*: single chain variable fragment; APH: thermophilic acylpeptide hydrolase; GAS: GNRs-APH-*scFv*; mAbs: monoclonal antibodies; NIR: near-infrared; SP: senile plaques; NFT: neurofibrillary tangles; NPs: nanoparticles; IDE: insulin-degrading enzyme; ADEs: amyloid-degrading enzymes; HFIP: 1,1,1,3,3,3-hexafluoro-2-propanol; CTAB: hexadecyltrimethylammonium bromide; ThT: thioflavin T; LSPR: localized surface plasmon resonance; TMB: 3,3',5,5'-tetramethylbenzidine; TEM: transmission electron microscopy; FTIR: fourier transform infrared spectroscopy; MTT: 3-(4,5-dimethylthiazol-2-yl)-2,5-

diphenyltetrazolium bromide; tricine-SDS-PAGE: tricine-sodium dodecyl sulfate-polyacrylamide gel electrophoresis; DMSO: dimethyl sulfoxide; *C.elegans*: *Caenorhabditis elegans*; *E.coli*: *Escherichia coli*; NGM: nematode growth media; HPLC-MS: high-performance liquid chromatography- mass spectrometry; ROS: reactive oxygen species; CD: Cyclic Dichroism.

## Supplementary Material

Supplementary figures.

<http://www.thno.org/v09p2268s1.pdf>

Supplementary video 1.

<http://www.thno.org/v09p2268s2.mpg>

Supplementary video 2.

<http://www.thno.org/v09p2268s3.mpg>

Supplementary video 3.

<http://www.thno.org/v09p2268s4.mpg>

Supplementary video 4.

<http://www.thno.org/v09p2268s5.mpg>

## Acknowledgements

### Author Contributions

D.L. designed and performed the experiments (A $\beta$  preparation, ThT assay, A $\beta$  toxicity inhibition assay, *C. elegans* paralysis assay), analyzed the data and edited the manuscript. W.L. designed and performed the experiments (A $\beta$  preparation, GAS synthesis, TEM assay, A $\beta$ -mediated peroxidase activity measurements, *C. elegans* paralysis assay), analyzed the data and wrote the manuscript. X.J. performed the experiment (A $\beta$  toxicity inhibition assay). S.B. performed the experiment (*C. elegans* maintenance and treatment). J.L., X.L., Y.S., Z.K. performed the experiments (GNRs synthesis, protein expression and purification). W.K., R.G. and Y.S. supervised the study, and reviewed, and edited the manuscript.

### Funding

The current work was supported by the National Natural Science Foundation of China (Grant no. 31770996 & 21778021), Industrial Technology Research and Development Projects of Jilin Province Development and Reform Commission (Grant no. 2014Y081), Science and Technology Enterprise Technology Innovation Fund of the Science and Technology Department of Jiangsu Province (Grant no. BC2015065), and Program for Jilin University Science and Technology Innovative Research Team (JLUSTIRT) (No. 2017TD-05).

## Competing Interests

The authors have declared that no competing interest exists.

## References

- Brookmeyer R, Johnson E, Ziegler-Graham K, Arrighi HM. Forecasting the global burden of Alzheimer's disease. *Alzheimers Dement*. 2007; 3: 186-91.
- Kosik KS. Alzheimer's disease: a cell biological perspective. *Science*. 1992; 256: 780-3.
- Brendel M, Jaworska A, Overhoff f, Blume T, Probst F, Gildehaus FJ, et al. Efficacy of chronic BACE1 inhibition in P52APP mice depends on the regional A $\beta$  deposition rate and plaque burden at treatment initiation. *Theranostics*. 2018; 4957-68.
- Hamley IW. The amyloid beta peptide: a chemist's perspective. Role in Alzheimer's and fibrillization. *Chem Rev*. 2012; 112: 5147-92.
- Li M, Howson SE, Dong K, Gao N, Ren J, Scott P, et al. Chiral metallohelical complexes enantioselectively target amyloid  $\beta$  for treating Alzheimer's disease. *J Am Chem Soc*. 2014; 136: 11655-63.
- Tanzi RE, Bertram L. Twenty years of the Alzheimer's disease amyloid hypothesis: a genetic perspective. *Cell*. 2005; 120: 545-55.
- Bateman RJ, Munsell LY, Morris JC, Swarm R, Yarasheski KE, Holtzman DM. Human amyloid-beta synthesis and clearance rates as measured in cerebrospinal fluid in vivo. *Nat Med*. 2006; 7: 856-61.
- Viola KL, Klein WL. Amyloid  $\beta$  oligomers in Alzheimer's disease pathogenesis, treatment, and diagnosis. *Acta Neuropathol*. 2015; 129: 183-206.
- He G, Luo W, Li P, Remmers C, Netzer WJ, Hendrick J, et al. Gamma-secretase activating protein is a therapeutic target for Alzheimer's disease. *Nature*. 2010; 2: 95-8.
- Yoo SI, Yang M, Brender JR, Subramanian V, Sun K, Joo NE, et al. Inhibition of amyloid peptide fibrillation by inorganic nanoparticles: functional similarities with proteins. *Angew Chem Int Ed Engl*. 2011; 50: 5110-5.
- Miners JS, Baig S, Palmer J, Palmer LE, Kehoe PG, Love S. Abeta-degrading enzymes in Alzheimer's disease. *Brain Pathol*. 2008; 18: 240-52.
- Miners JS, Barua N, Kehoe PG, Gill S, Love S. A $\beta$ -degrading enzymes: potential for treatment of Alzheimer disease. *J Neuropathol Exp Neurol*. 2011; 11: 944-59.
- Agadjanyan MG, Petrovsky N, Ghochikyan A. A fresh perspective from immunologists and vaccine researchers: active vaccination strategies to prevent and reverse Alzheimer's disease. *Alzheimers Dement*. 2015; 11: 1246-59.
- Bard F, Barbour R, Cannon C, Carretto R, Fox M, Games D, et al. Epitope and isotype specificities of antibodies to beta -amyloid peptide for protection against Alzheimer's disease-like neuropathology. *Proc Natl Acad Sci U S A*. 2003; 100: 2023-8.
- Cabaleiro-Lago C, Quinlan-Pluck F, Lynch I, Lindman S, Minogue AM, Thulin E, et al. Inhibition of amyloid beta protein fibrillation by polymeric nanoparticles. *J Am Chem Soc*. 2008; 130: 15437-43.
- Xia N, Zhou B, Huang N, Jiang M, Zhang J, Liu L. Visual and fluorescent assays for selective detection of beta-amyloid oligomers based on the inner filter effect of gold nanoparticles on the fluorescence of CdTe quantum dots. *Biosens Bioelectron*. 2016; 85: 625-32.
- Guan Y, Li M, Dong K, Gao N, Ren J, Zheng Y, et al. Ceria/POMs hybrid nanoparticles as a mimicking metalloproteinase for treatment of neurotoxicity of amyloid- $\beta$  peptide. *Biomaterials* 2016; 98: 92-102.
- Sahni JK, Doggui S, Ali J, Baboota S, Dao L, Ramassamy C. Neurotherapeutic applications of nanoparticles in Alzheimer's disease. *J Control Release* 2011; 152: 208-31.
- Amiri H, Saeidi K, Borhani P, Manafirad A, Ghavami M, Zerbi V. Alzheimer's disease: pathophysiology and applications of magnetic nanoparticles as MRI theranostic agents. *ACS Chem Neurosci*. 2013; 4: 1417-29.
- Foguel D, Suarez MC, Ferrão-Gonzales AD, Porto TC, Palmieri L, Einsiedler CM, et al. Dissociation of amyloid fibrils of alpha-synuclein and transthyretin by pressure reveals their reversible nature and the formation of water-excluded cavities. *Proc Natl Acad Sci U S A*. 2003; 17: 9831-6.
- Yang L, Tseng YT, Suo G, Chen L, Yu J, Chiu W, et al. Photothermal therapeutic response of cancer cells to aptamer-gold nanoparticle-hybridized graphene oxide under NIR illumination. *ACS Appl Mater Interfaces*. 2015; 7: 5097-106.
- Chen Q, Xu L, Liang C, Wang C, Peng R, Liu Z. Photothermal therapy with immune-adjuvant nanoparticles together with checkpoint blockade for effective cancer immunotherapy. *Nat Commun*. 2016; 7: 13193.
- Li M, Yang J, Ren J, Qu K, Qu X. Using graphene oxide high near-infrared absorbance for photothermal treatment of Alzheimer's disease. *Adv Mater*. 2012; 24: 1722-8.
- Wust P, Hildebrandt B, Sreenivasa G, Rau B, Gellermann J, Riess H, et al. Hyperthermia in combined treatment of cancer. *Lancet Oncol*. 2002; 3: 487-97.
- Guo L, Yan DD, Yang D, Li Y, Wang X, Zalewski O, et al. Combinatorial photothermal and immuno cancer therapy using chitosan-coated hollow copper sulfide nanoparticles. *ACS Nano*. 2014; 8: 5670-81.
- Ghosh S, Dutta S, Gomes E, Carroll D, D'Agostino R Jr, Olson J, et al. Increased heating efficiency and selective thermal ablation of malignant tissue with DNA-encased multiwalled carbon nanotubes. *ACS Nano*. 2009; 3: 2667-73.
- Hirsch LR, Stafford RJ, Bankson JA, Sershen SR, Rivera B, Price RE, et al. Nanoshell-mediated near-infrared thermal therapy of tumors under magnetic resonance guidance. *Proc Natl Acad Sci U S A*. 2003; 100: 13549-54.
- Pramanik D, Dey SG. Active site environment of heme-bound amyloid  $\beta$  peptide associated with Alzheimer's disease. *J Am Chem Soc*. 2011; 133: 81-7.

29. Atamna H, Boyle K. Amyloid-beta peptide binds with heme to form a peroxidase: relationship to the cytopathologies of Alzheimer's disease. *Proc Natl Acad Sci U S A* 2006; 103: 3381-6.
30. Li R, Gao R. Expression and characterization of a thermostable acyl-peptide releasing enzyme ST0779 from *Sulfolobus tokodaii*. *Chem Res Chin Univ*. 2012; 28: 851-5.
31. Han KH, Arlian BM, Macauley MS, Paulson JC, Lerner RA. Migration-based selections of antibodies that convert bone marrow into trafficking microglia-like cells that reduce brain amyloid  $\beta$ . *Proc Natl Acad Sci U S A*. 2018; 115: E372-E381.
32. Fu L, Li Y, Hu Y, Zheng Y, Yu B, Zhang H, et al. Norovirus P particle-based active A $\beta$  immunotherapy elicits sufficient immunogenicity and improves cognitive capacity in a mouse model of Alzheimer's disease. *Sci Rep*. 2017; 7: 41041.
33. El-Sayed A, Bernhard W, Barreto K, Gonzalez C, Hill W, Pastushok L, et al. Evaluation of antibody fragment properties for near-infrared fluorescence imaging of HER3-positive cancer xenografts. *Theranostics*. 2018; 8: 4856-69.
34. Krol S, Macrez R, Docagne F, Defer G, Laurent S, Rahman M, et al. Therapeutic benefits from nanoparticles: the potential significance of nanoscience in diseases with compromise to the blood brain barrier. *Chem Rev*. 2013; 113: 1877-903.
35. Hinterwirth H, Kappel S, Waitz T, Prohaska T, Lindner W, Lammerhofer M. Quantifying thiol ligand density of self-assembled monolayers on gold nanoparticles by inductively coupled plasma-mass spectrometry. *ACS Nano*. 2013; 7: 1129-36.
36. Singh AK, Senapati D, Wang S, Griffin J, Neely A, Candice P, et al. Gold nanorod based selective identification of *Escherichia coli* bacteria using two-photon rayleigh scattering spectroscopy. *ACS Nano*. 2009; 3: 1906-12.
37. Li M, Guan Y, Zhao A, Ren J, Qu X. Using multifunctional peptide conjugated Au nanorods for monitoring  $\beta$ -amyloid aggregation and chemo-photothermal treatment of Alzheimer's disease. *Theranostics*. 2017; 7: 2996-3006.
38. Yang X, Liu X, Liu Z, Pu F, Ren J, Qu X. Near-infrared light-triggered, targeted drug delivery to cancer cells by aptamer gated nanovehicles. *Adv Mater*. 2012; 24: 2890-5.
39. Blankschien MD, Pretzer LA, Huschka R, Halas NJ, Gonzalez R, Wong MS. Light-triggered biocatalysis using thermophilic enzyme-gold nanoparticle complexes. *ACS Nano*. 2013; 7: 654-63.
40. Sudhakar S, Kalipilai P, Santhosh PB, Mani E. Role of surface charge of inhibitors on amyloid beta fibrillation. *J Phys Chem C*. 2017; 121: 6339-48.
41. Ramesh NK, Sudhakar S, Mani E. Modeling of the inhibitory effect of nanoparticles on amyloid  $\beta$  fibrillation. *Langmuir*. 2018; 34: 4004-12.
42. Sudhakar S, Santhosh B, Mani E. Dual role of gold nanorods: inhibition and dissolution of A $\beta$  fibrils induced by near IR laser. *ACS Chem Neurosci*. 2017; 8: 2325-34.
43. Hyung SJ, DeToma AS, Brender JR, Lee S, Vivekanandan S, Kochi A, et al. Insights into anti-amyloidogenic properties of the green tea extract (-)-epigallocatechin-3-gallate toward metal-associated amyloid- $\beta$  species. *Proc Natl Acad Sci U S A*. 2013; 110: 3743-8.
44. Yu C, Irudayaraj J. Multiplex biosensor using gold nanorods. *Anal Chem*. 2007; 79: 572-9.
45. Wang J, Zhao C, Zhao A, Li M, Ren J, Qu X. New insights in amyloid beta interactions with human telomerase. *J Am Chem Soc*. 2015; 137: 1213-9.
46. Pramanik D, Ghosh C, Dey SG. Heme-Cu bound A $\beta$  peptides: spectroscopic characterization, reactivity, and relevance to Alzheimer's disease. *J Am Chem Soc*. 2011; 133: 15545-52.